# Corrosion of Heat Transfer Materials by Potassium-Contaminated Ilmenite Bed Particles in Chemical-Looping Combustion of Biomass

Eriksson, Jan-Erik; Zevenhoven, Maria; Yrjas, Patrik; Brink, Anders; Hupa, Leena

*Published in:*
Energies

*DOI:*
10.3390/en15082740

Published: 01/04/2022

*Document Version*
Final published version

*energies*

MDPI

*Article*

# Corrosion of Heat Transfer Materials by Potassium-Contaminated Ilmenite Bed Particles in Chemical-Looping Combustion of Biomass

**Jan-Erik Eriksson [1,*], Maria Zevenhoven [1], Patrik Yrjas [1], Anders Brink [2] and Leena Hupa [1]**

[1] Johan Gadolin Process Chemistry Centre, Åbo Akademi University, 20500 Turku, Finland; maria.zevenhoven@abo.fi (M.Z.); patrik.yrjas@abo.fi (P.Y.); leena.hupa@abo.fi (L.H.)
[2] Laboratory of Process and Systems Engineering, Åbo Akademi University, 20500 Turku, Finland; anders.brink@abo.fi
* Correspondence: jan-erik.eriksson@abo.fi

**Abstract:** This study discusses the potential corrosion of boiler materials in chemical-looping combustion (CLC) of biomass. The CLC of biomass has the potential to negative $CO_2$ emission in heat and power production. Biomass fuels, however, typically contain compounds of alkali metals, especially potassium and chloride, which may lead to the corrosion of heat-transfer surfaces in the reactors. The influence of potassium-contaminated ilmenite bed material deposits on the corrosion of seven heat transfer materials used in the air and fuel reactors in CLC was studied using one-week lab-scale experiments. Samples with KCl and without any deposit were used as references. After the exposure, the cross-sectional surfaces of the metals were analyzed with SEM/EDX. The results suggested that potassium-contaminated ilmenite might lead to minor corrosion of all studied materials under the oxidizing conditions simulating the air reactor, i.e., 700 °C and dry air. Under reducing fuel reactor conditions, i.e., 450 °C and 550 °C and 50/50 $CO_2/H_2O$, corrosion was observed on ferritic steels, especially in the presence of HCl and with KCl deposit. In contrast, samples with uncontaminated and potassium-contaminated ilmenite deposits did not significantly differ from the samples without any deposit. Minor corrosion of ferritic steels was observed at 450 °C, while at 550 °C, the corrosion was more significant. The results suggested that ferritic steels are not suitable for the fuel reactor. Austenitic and nickel-based alloys did not corrode under the test conditions used in this work.

**Keywords:** chemical looping combustion; ilmenite; corrosion; heat transfer



**Citation:** Eriksson, J.-E.; Zevenhoven, M.; Yrjas, P.; Brink, A.; Hupa, L. Corrosion of Heat Transfer Materials by Potassium-Contaminated Ilmenite Bed Particles in Chemical-Looping Combustion of Biomass. *Energies* **2022**, *15*, 2740. https://doi.org/10.3390/en15082740

Academic Editor: Fernando Rubiera González

Received: 1 March 2022
Accepted: 4 April 2022
Published: 8 April 2022



## 1. Introduction

Biomass combustion continues to be a feasible option for decreasing the emission of $CO_2$ into the atmosphere. However, satisfying the requirement in the Paris Agreement to limit the global earth atmosphere temperature increase below 1.5 °C compared to the preindustrial times calls for changes in combustion technologies [1]. An option could be to capture and store or utilize $CO_2$ emitted from biomass combustion (BECCUSS) [2]. In traditional combustion technologies, $CO_2$ emissions are diluted with other flue gases, such as air nitrogen. In chemical looping combustion (CLC), the dilution is avoided since the flue gas is concentrated in $CO_2$ [3].

CLC consists of two intertwined reactors, i.e., an air reactor and a fuel reactor. The bed material used as an oxygen carrier in the air reactor is oxidized by air. The fuel, biomass, is oxidized through reactions with the oxidized bed material in the fuel reactor, consequently reducing the bed material. As the bed material consists of oxides of redox metals, the shift between different oxidation states enables oxygen transport between the two reactors. The bed material reacts with gaseous fuel components that form when the solid fuel pyrolyzes in the fuel reactor. Steam and the produced flue gases can be used as fluidizing agents in the fuel reactor. In this way, char produced in the pyrolysis process is gasified by the

fluidizing media. CO and $H_2$ produced in the gasification process react with the oxygen carrier to $CO_2$ and $H_2O$. The temperature in the fuel reactor is slightly lower than in the air reactor, i.e., 760–820 °C and 840–1000 °C, respectively. The principle of CLC is presented in Figure 1.

Lewis and Gilland initially proposed CLC for producing pure $CO_2$ in 1954 [4], and the method has been improved over the years [5–7]. Today, the focus of Chemical Looping is laid on combustion (CLC), shifting from fossil fuels to biomass fuels [7–12]. Using a renewable fuel, such as biomass, carbon capture, and sequestration potential may lead to negative $CO_2$ emissions from CLC [13].

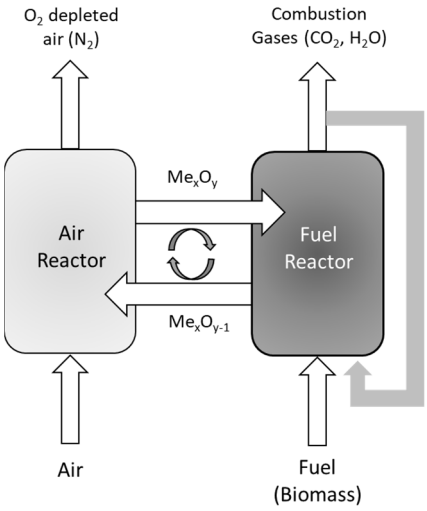


**Figure 1.** The simplified main principle of chemical-looping combustion. Two designated reactors where oxygen carrier is respectively oxidized and reduced.

Traditional heat exchanger designs could be used to recover heat from the hot air in the air reactor. Minor corrosion may be expected here since the flue gas stream from the fuel reactor and air stream remain separated. No corrosion-inducing elements from the fuel, such as chlorine, enter the air reactor. However, a small slipstream from the fuel reactor, e.g., as ash in the bed material, may be expected in practice.

Recently, a second-generation CLC setup was proposed by Alstom [14]. This setup allows two sets of heat exchangers to be used, one in either reactor. This raises the boiler efficiency considerably.

One of the oxygen carriers thoroughly studied is ilmenite, i.e., iron–titanium oxide, $FeTiO_3$ [15–19]. Ilmenite can be considered a benchmark oxygen carrier. Based on the iron content of ilmenite, the reduction capacity is theoretically limited to 5 wt %. The reduction can be described by the reaction below (1), where the oxidized phase is pseudobrookite and the reduced phase is ilmenite:

$$Fe_2O_3{\cdot}TiO_2\ (s) + TiO_2(s) + CO(g) \rightarrow 2FeO{\cdot}TiO_2(s) + CO_2(g) \quad (1)$$

The redox reactions of Fe have been described in detail by Leion et al. [19]. The process circulates between the reduced form ilmenite, $FeTiO_3$, and the oxidized form $Fe_2O_3{\cdot}TiO_2$ + $TiO_2$.

The use of biomass as fuel in CLC can be considered challenging. Biomass-based fuels are chemically heterogeneous, and their quality variations are large [20]. The ash-forming matter in biomass contains typically high amounts of Si, K, and Ca. Especially K-containing compounds may be reactive and lead to deposit formation or corrosion [21–24].

In conditions relevant to biomass combustion, different mechanisms for corrosion, i.e., chlorine-induced active oxidation, have been proposed and summarized by, e.g., Elger [25]:

1. Gaseous chlorine-induced corrosion, where gaseous HCl or $Cl_2$ diffuses to and reacts with a metal surface forming iron chloride ($FeCl_x$). These chlorides may vaporize and diffuse to the surface towards a higher oxygen partial pressure, where it oxidizes forming a Fe-rich oxide layer at the metal–gas interface, releasing chlorine, which could react again with iron and thus, act as an intermediate or a catalyst in the corrosion process [26,27].
2. Alkali chloride-induced corrosion. KCl may react (directly) with iron in low-alloy steels, forming iron chloride. As iron chloride then diffuses towards a higher oxygen partial pressure and eventually oxidizes, the released chlorine (gas) may continue the corrosion process in a similar way as described above [28,29].

In the case of high-alloy steels, it has been proposed that the protective $Cr_2O_3$ layer also can react with KCl, resulting in $K_2CrO_4$ formation, thus losing the protective properties of the layer [29,30]. Simultaneously with $K_2CrO_4$ formation, the released chlorine could sustain the corrosion process as described above.

3. Molten salt corrosion. This third mechanism may involve the interaction between the metal oxide scale and the molten salt at the oxide–salt interface leading to fast corrosion [31].

The form of chlorine diffusing into the steel and the details of the chlorine cycle are not fully clear. Chlorine has been suggested to be either in the form of $Cl_2$ or HCl.

Another alternative for chlorine transportation is an electrochemical mechanism, which suggests that chloride ions diffuse to the metal–oxide interface instead of a gas transport of chlorine through the oxide scale [26,32].

In power boilers firing biomass, corrosion is often induced by the formation of corrosive alkali chloride deposits on superheaters operating at 400 to 600 °C. The alkali chloride-induced corrosion of superheaters has been explained by the consecutive mechanisms described above.

As of today, corrosion in biomass-fired CLC has not been studied. However, Lyngfelt assumed that corrosion would not pose a problem [7]. This assumption may be valid but has not been proven for a first-generation CLC setup, where heat exchangers are only located in the air reactor, with no $KCl/HCl/Cl_2$ from the fuel reactor. If biomass-based fuels were fired in a second-generation CLC, heat exchangers would also be situated in the fuel reactor area.

The study presented here aims to show whether corrosion can be expected to be a significant problem in the second-generation biomass-fired CLC. Hereto, 95 laboratory-scale experiments were designed imitating air reactor and fuel reactor conditions. In the past, similar lab-scale corrosion experiments carried out in controlled atmospheres have produced useful results that have been translated to large-scale processes [22–24,30,33–35].

Laboratory-scale corrosion tests were performed using seven materials (ferritic and austenitic steels and nickel-based alloys). The sample surfaces were in contact with fresh oxygen carrier material, oxygen carrier material that had been in contact with KCl, or KCl in a heated gaseous atmosphere resembling CLC conditions.

## 2. Materials and Methods

### *2.1. Materials*

Analytical grade KCl by Sigma Aldrich was used, mimicking the most critical ash component when considering corrosion in a biomass-fired boiler.

The oxygen carrier used was Norwegian rock ilmenite provided by Titania AS, Norway. The mean particle size of the as-received ilmenite particles was 300 µm. Heat treatment, i.e., activation of ilmenite, was carried out in an electrically heated tube furnace at 950 °C in air.

The reaction of potassium-containing ash with ilmenite was mimicked by adding KCl to a total content of 4 wt% K to the heat-treated ilmenite. This concentration was based on the amount of accumulated potassium found in the bed after three days of operation in a

semi-industrial biomass CFB boiler operated with ilmenite under OCAC (Oxygen Carrier Aided Combustion) conditions) [36].

Hereafter, the mixture was treated at 850 °C under a reducing atmosphere containing 5% CO, 45% $N_2$, and 50% $H_2O$ in a tube furnace for 6 h. The reduced material, K-ilmenite$_{red}$, was used for corrosion experiments simulating conditions in the fuel reactor. Part of the reduced material was re-oxidized at 950 °C, imitating the entrance of bed material into the air reactor. The re-oxidized material, K-ilmenite$_{ox}$, was used for corrosion tests under oxidizing conditions.

After cooling, potassium and chlorine contents of the potassium doped sample, K-ilmenite$_{red}$, were analyzed with SEM-EDX. The elemental composition of the samples was determined by gluing the material on carbon tape and analyzing it with a scanning electron microscope equipped with an energy-dispersive X-ray (SEM-EDXA, Leo 1530 Gemini, Thermo Scientific UltraDry SDD X-ray detector).

The heat transfer materials chosen to simulate the air reactor (A metals) were austenitic stainless steels TP347, TP310, Sanicro28, and nickel-based alloys HRN11 and Inconel617, while the materials (F metals) chosen for the fuel reactor were the ferritic steels 10CrMo9-10, X10, and austenitic stainless steels TP347, TP310, and Sanicro28. Thus, three same austenitic plates of stainless steel were studied for both reactors. All tested materials were delivered by different Finnish boiler manufacturers. The elemental distribution of the alloy compositions of the metals is presented in Figure 2.

The metal test pieces were pre-treated as described by Skrifvars et al. [22]. Hereto, the metals were cut to ~20 × 20 mm pieces with a thickness of ~5–10 mm, then hand polished with gradually finer sandpapers. The final touch was made with grade p1000 sandpaper and ethanol. Hereafter, the pieces were prepared for exposure to deposits, i.e., salts, ilmenite, or K-ilmenite, using the procedure described by Bankiewicz et al. [33]. A fireproof sealer was applied along the edges of the metal samples to give a shallow pool for the deposits. Then, the metal pieces were pre-oxidized in air at 200 °C for 24 h.

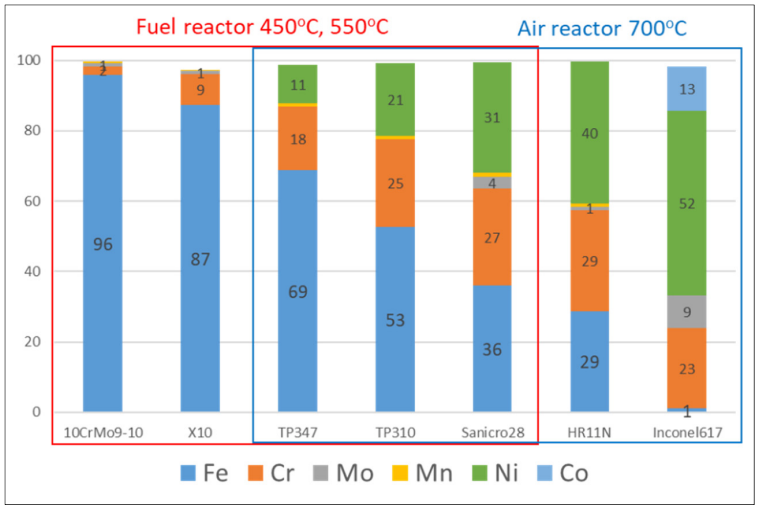


**Figure 2.** Nominal composition (wt%) of the tested boiler materials. Only the main components are indicated. The red and blue rectangular borders show the materials tested at 450 °C or 550 °C under fuel reactor conditions and 700 °C under air reactor conditions.

### *2.2. Corrosion Experiments*

In addition to blank tests with no deposit, four different deposit types were used in the experiments: (1) heat-treated ilmenite ("activated ilmenite"); (2,3) potassium chloride-contaminated heat-treated ilmenite, which was either reduced or re-oxidized ("K-ilmenite$_{red/ox}$"); and (4) samples with pure potassium chloride ("KCl"). KCl simulated the most extreme situation where some of the KCl in the biomass ash has not reacted with the ilmenite but is found in the fly ash.

The corrosion experiments were conducted in three series under different atmospheres, i.e., 50/50 $CO_2/H_2O$ imitating conditions in the fuel reactor, 50/50 $CO_2/H_2O$ with 500 ppm HCl resembling harsh conditions in the fuel reactor, and air mimicking conditions in the air reactor. The total exposure time was 168 h at each target temperature.

Under reducing conditions, the samples were treated in a horizontal Carbolite tube furnace equipped with an alumina inner tube. A gas-tight quartz tube with gas inlets and outlets was inserted into the inner alumina tube of the furnace. The quartz tube was connected to a steam generator. This setup enabled the introduction of controlled artificial atmospheres in the tube reactor (Figure 3a).

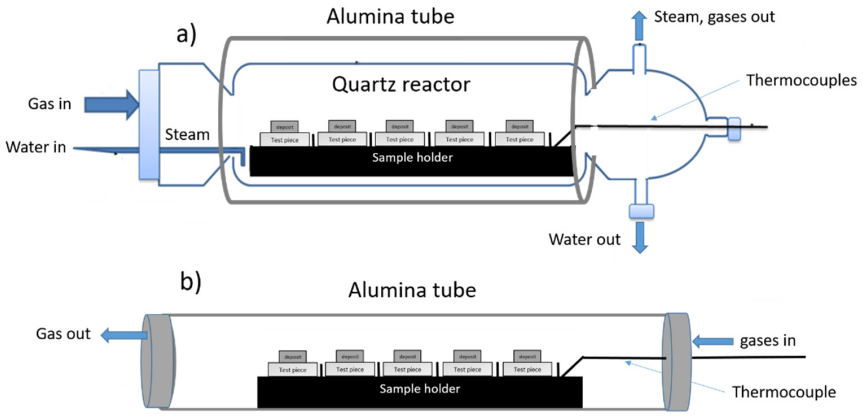


**Figure 3.** Quartz reactor and alumina tube used in experiments under (**a**) reducing and (**b**) oxidizing conditions.

Two different reducing atmospheres, with a total gas flow of 2 L/min at NTP, were used: 50/50 $CO_2/H_2O$ and 50/50 $CO_2/H_2O$ + 500 ppm HCl. The fuel reactor temperature was set to either 450 °C or 550 °C, i.e., typical temperatures for heat exchanger surfaces in biomass-fired boilers. The test pieces were inserted into the furnace on a ceramic sample holder at room temperature. The heating to the target temperature was controlled manually with thermocouples connected to the sample holder. While heating from room temperature to 200 °C, a gas flow of 1 L/min $CO_2$ mixed with 1 L/min of $N_2$, balancing the total flow, was used. Hereafter, $N_2$ was replaced by steam or a mixture of steam with HCl, and the furnace was heated to the target temperature, 450 °C or 550 °C.

Under oxidizing conditions, the experiments were carried out in a similar arrangement. However, the inner quartz tube was not used. The setup is shown in Figure 3b. A constant flow of 1 L/min at NTP of dry air was used. The test pieces with deposits were inserted into the hot furnace using a cast iron sample holder [33]. The temperature was adjusted manually to the target temperature of 700 °C. Five thermocouples located in the sample holder between each test piece were used to monitor the temperature. No reference deposit of pure KCl was tested under air reactor conditions. In CLC, KCl is not expected to enter the air reactor.

The experimental matrix of this study is presented in Table 1. In total, 95 samples were studied.

**Table 1.** Summary of test conditions. A—metals tested for air reactor; F for fuel reactor.

| Deposit | Oxidizing Conditions | Reducing Conditions | |
|---|---|---|---|
| | 700 °C<br>Dry Air | 450 °C<br>50/50 $CO_2/H_20$ | 550 °C<br>50/50 $CO_2/H_2O$ + 500 ppm HCl |
| No deposit | A | F | F |
| Ilmenite | A | F | F |
| K-ilmenite$_{ox}$ | A | | |
| K-Ilmenite$_{red}$ | | F | F |
| KCl | — | F | F |

### *2.3. Analyses*

After cooling to room temperature, a small amount of epoxy resin was put over the samples and left to harden overnight. Next, the samples were cast sideways in epoxy resin in molds and left to harden for 12 h. Similar to Bankiewicz et al. [33], the epoxy-embedded pieces were cut to expose the cross-sectional surface. The surface was polished and carbon-coated for imaging and analysis. For the elemental composition analysis and the cross-sectional images, a scanning electron microscope equipped with an energy dispersive X-ray (SEM-EDXA, Leo 1530 Gemini, Thermo Scientific UltraDry SDD X-ray detector) was used.

The thickness of a corrosion layer was determined from colored images using image analysis. The SEM images were colored to show the epoxy resin and surface deposit in blue, the unoxidized metal in red, and the oxide layer in green. The oxide layer thickness and distribution were calculated automatically from the colored image with analyzing software. A 4 mm wide colored panoramic SEM image was analyzed using 10,000 thickness measurement points by self-made software. The corrosion layer thickness was calculated from these measurements automatically. As a result, the mean and maximum corrosion layer thickness was obtained.

## 3. Results

### *3.1. Pretreatment of Ilmenite*

During the heat-treatment of ilmenite, the particles were activated. Thus, ilmenite was oxidized, and an Fe-rich layer formed at the outside of the particles optimizing the oxygen carrier capacity of the particles. This segregation of Ti and Fe has been shown in numerous papers [36–39].

The heat-treated ilmenite mixed with 4 wt% K (as KCl) had been reduced in a tube furnace in a moist atmosphere producing "K-ilmenite$_{red}$". SEM-EDX analyses of the surface of the particles confirmed enrichment of some 4 wt% potassium at the surface. Potassium on and in particles is likely potassium titanate, according to reactions 2 and 3 suggested by Corcoran et al. and Hildor et al. [36,39]. Figure 4 shows a back-scattered SEM image and elemental maps of K, Ti, and Fe, respectively, shown in green, red, and blue:

$$KCl(s) + H_2O \rightarrow KCl(g) + KOH(l) + HCl(g) \quad (2)$$

$$\text{ilmenite} + KOH(l) \rightarrow \text{K-titanate}(s) + KOH(g) \quad (3)$$

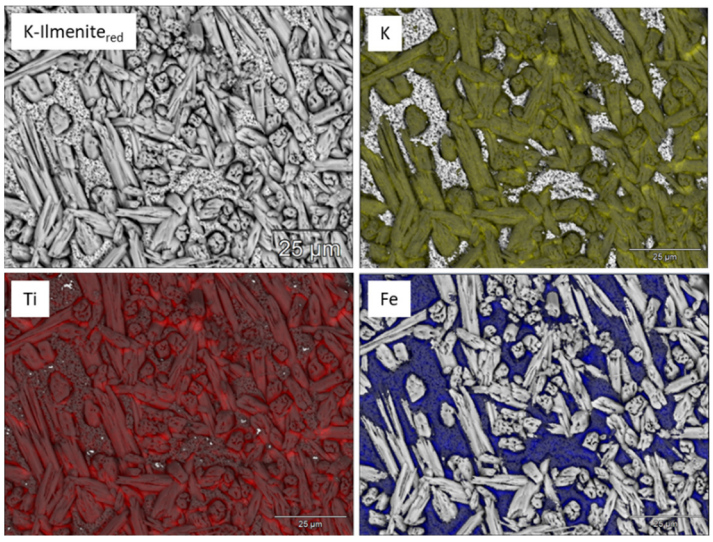


**Figure 4.** Back-scattered SEM image and elemental maps of K-Ilmenite$_{red}$ showing K (green), Ti (red), and Fe (blue). K was associated with titanium only.

In the CLC process, the reduced ilmenite that has reacted with potassium in the fuel reactor will be transported to the air reactor and oxidized thereafter. In this work, the reduced K-ilmenite$_{red}$ was re-oxidized under similar conditions as in a CLC air reactor (950 °C in air for 6 h). SEM images of re-oxidized K-ilmenite (K-ilmenite$_{ox}$) are shown below in Figure 5.

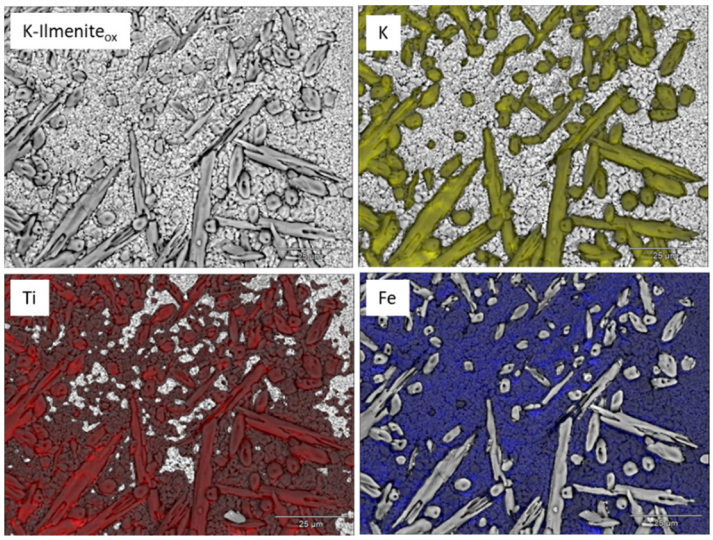


**Figure 5.** Back-scattered SEM image and elemental maps of oxidized K-Ilmenite$_{ox}$ showing K (green), Ti (red), and Fe (blue).

The SEM-EDX analyses of the surface of the oxidized K-ilmenite$_{ox}$ particles showed that the potassium enrichment remained after re-oxidization and that a stable phase of K-titanate was present.

### *3.2. Corrosion under Reducing Conditions*

Figure 6 shows an example of the image analysis of ferritic steel 10CrMo9-10 exposed to K-ilmenite$_{red}$, at 550 °C, in $CO_2/H_2O$ + HCl. The upper image shows the original back-scattered SEM image, and the lower the colored SEM image. The epoxy resin and surface deposit are shown in blue, the unoxidized metal in red, and the oxide layer in green. The figure shows a 4 mm wide image of the surface: the original back-scattered image of the K-ilmenite$_{red}$ particles on the sample surface and the colored image showing the metal surface with the corrosion layer.

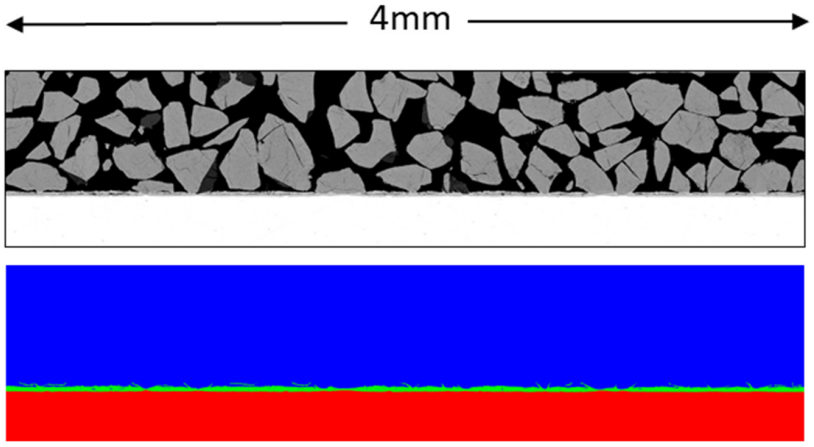


**Figure 6.** An example showing the back-scattered SEM image of 10CrMo9-10 cross-section (upper) and (lower) the colored cross-section of the same image showing the green-colored oxide layer between the metal (red) and deposit-epoxy mixture (blue).

Figure 7 shows the distribution curve of the corrosion layer thickness for 10CrMo9-10 covered with a KCl deposit treated at 550 °C in a steam atmosphere. The oxide layer thickness was determined from the colored SEM image. The vertical lines shown in Figure 7 indicate the mean, median, maximum, and minimum thickness of the oxide layer. Typically, the distribution was quite wide since the oxide layer was not uniform. Other metals' distribution profiles are given in the supplementary material (Figures S1–S6).

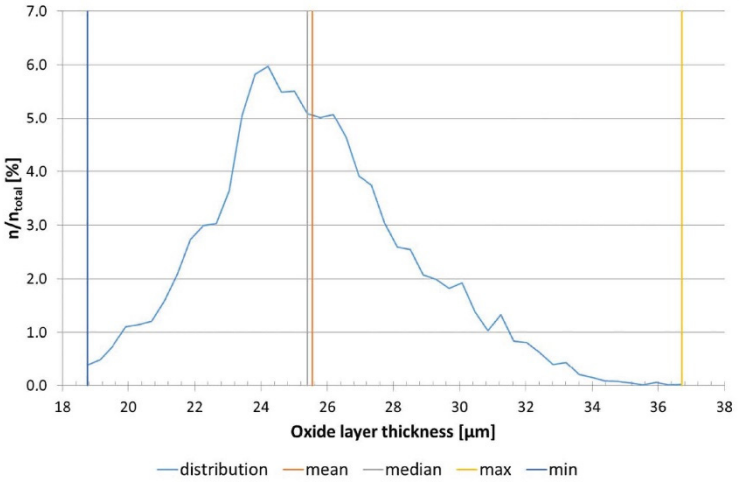


**Figure 7.** Oxide layer thickness distribution curve and $t_{mean}$, $t_{median}$, $t_{max}$, and $t_{min}$ of a single corrosion test with 10CrMo9-10 covered with a KCl deposit treated at 550 °C in a steam atmosphere. ($n_{total}$ is 10,000).

Figure 8 shows the corrosion layer mean thickness values measured on the samples after the experiments carried out under reducing conditions, under 50/50 $CO_2/H_2O$ and 50/50 $CO_2/H_2O$ + 500 ppm HCl atmospheres at 450 °C and 550 °C.

Under reducing conditions at 550 °C, significant corrosion was seen for all experiments with 10CrMo9-10 and X10, while no corrosion was detected for the austenitic stainless steels. In the presence of steam and HCl, the corrosion thickness was significantly higher and reached up to 40 µm for 10CrMo9-10 and X10, indicating that corrosion may occur if the heat is recovered from the fuel reactor with heat exchanger surface temperatures around 550 °C.

Figure 9 shows a back-scattered SEM image and elemental maps of 10CrMo9-10 covered with K-Ilmenite$_{red}$ after exposure at 550 °C in $CO_2/H_2O$. It can be seen that K is enriched at the K-ilmenite$_{red}$ surface, but K has not reacted with the metal surface enriched in Fe.

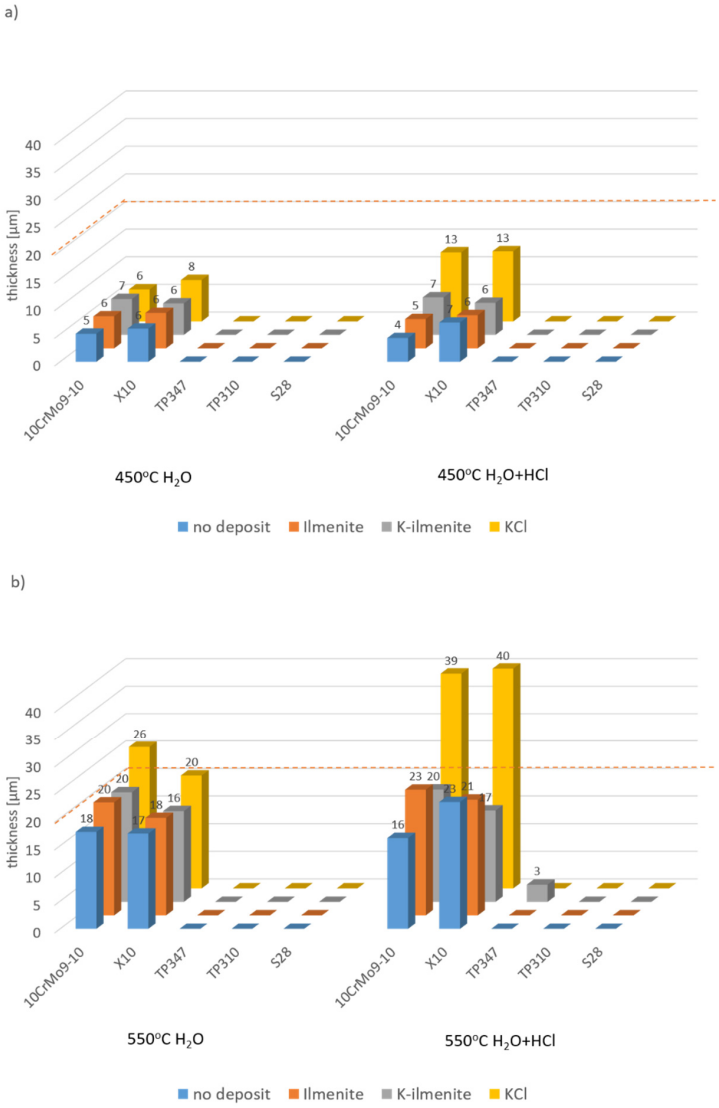


**Figure 8.** Mean thickness of oxide layers (µm) of samples exposed in (**a**) 50/50 $CO_2/H_2O$ and 50/50 $CO_2/H_2O$ + 500 ppm HCl at 450 °C and (**b**) 50/50 $CO_2/H_2O$ and 50/50 $CO_2/H_2O$ + 500 ppm HCl at 550 °C for 168 h. The dotted line indicates the 20 µm line above which corrosion is considered significant.

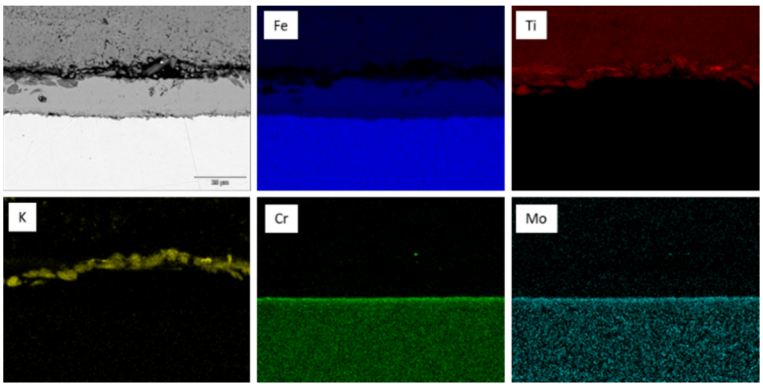


**Figure 9.** Back-scattered SEM image and elemental maps of 10CrMo9-10 covered with K-Ilmenite$_{red}$ after exposure at 550 °C in $CO_2/H_2O$ during 168 h showing K (yellow), Fe (blue), Ti (red), Cr (green), and Mo (cyan).

### *3.3. Corrosion under Oxidizing Conditions Mimicking Air Reactor Conditions*

Figure 10 shows the mean thickness of the corrosion layers formed under oxidizing conditions in air at 700 °C. The analyses show that under oxidizing conditions, a thin oxide layer formed on all metals in the presence of K-ilmenite$_{ox}$. No oxide layer was seen on samples without any deposit or with heat-treated ilmenite.

Figure 10 shows that the mean thickness of the corrosion layers measured for TP347 and TP310 at 700 °C was only 3.8 and 4.1 µm, respectively. Thus, these low-alloy steels showed minor corrosion. Corrosion of the high alloy steels remained negligible. When the corrosion layer thickness in the laboratory tests has remained below around 20 µm per week, the corrosion has not been considered significant [40].

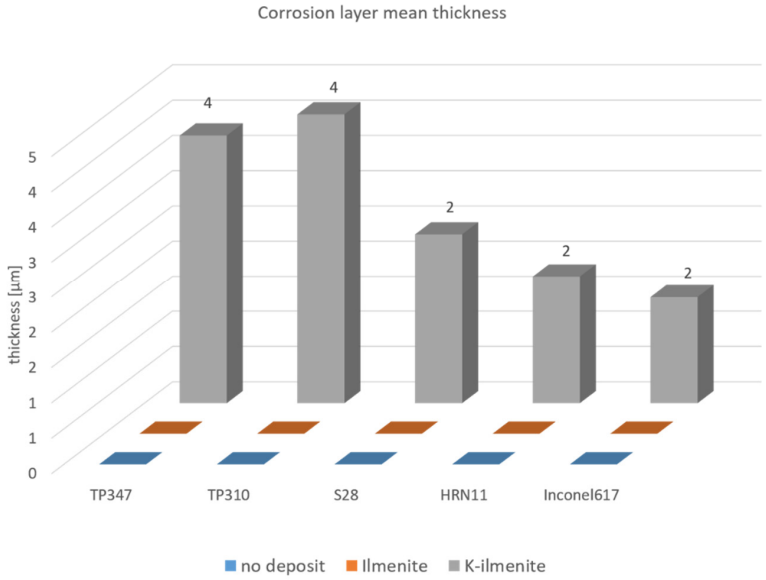


**Figure 10.** Mean thickness of oxide layer [µm] of samples exposed in dry air at 700 °C for 168 h.

Figure 11 shows one example of a back-scattered image from the SEM/EDX analysis and elemental maps from the experiment with TP347 covered with K-ilmenite$_{ox}$. The elemental maps show the appearance of the oxidized K-ilmenite particles on the sample surface and the presence of Fe, Ti, Cr, Ni, and K at the interface of an oxidized K-ilmenite particle and the metal surface after the experiment. The figure shows that deposit particles become separated from the surface when coating the samples in epoxy. As expected, K was enriched on the K-ilmenite$_{ox}$ particles. Ni and Fe were also enriched on the metal surface. In addition, some indications of Cr depletion from the surface could be identified.

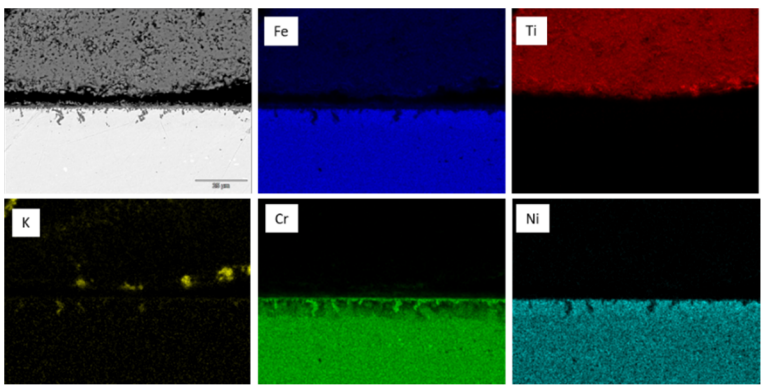


**Figure 11.** Back-scattered SEM image and elemental maps of TP347 covered with oxidized K-Ilmenite after exposure at 700 °C, in air during 168 h showing K (yellow), Fe (blue), Ti (red), Cr (green), and Mo (cyan).

## 4. Discussion

When thermally converting biomass, its inorganic matter and reactivity must be considered. Several biomasses contain potassium and chlorine; thus, KCl can be formed and released to the flue gas as a gaseous component or as molten fly ash leading to corrosion of heat exchanger surfaces [21–24]. In the second-generation CLC, KCl may deposit on heat exchanger surfaces in the fuel reactor and cause rapid corrosion. However, as described in this study and elsewhere [41–43], biomass ash compounds may interact with ilmenite bed material. This interaction is well known, and up to 4 wt% K has been found chemically bonded in ilmenite after 72 h of combustion using biomass fuels containing potassium [36].

It has been shown that potassium may react with the oxygen carrier ilmenite, forming K-titanates [36,39]. Thus, the presence of an oxygen carrier may indirectly decrease corrosion by capturing potassium.

This study suggested that KCl in the CLC fuel reactor might induce corrosion. In contrast, ilmenite was non-corrosive in all experiments. Potassium-doped/contaminated ilmenite, K-ilmenite, is a stable compound even after several redox cycles [36,39]. In the present study, K-ilmenite did not cause significant corrosion.

Under reducing conditions simulating the fuel reactor, the ferritic steels 10CrMo9-19 and X10 showed clear indications of corrosion at 450 °C, both with and without deposits. As expected, the thickest corrosion layer, 13 µm, was detected for ferritic steels 10CrMo9-10, and X10 when exposed to the reference deposit, pure KCl, under conditions where HCl was also present in the atmosphere. However, no apparent differences between the oxide layer thicknesses on the ferritic steels could be seen for the samples with deposits consisting of ilmenite, K-ilmenite$_{red}$, and the reference samples without a deposit.

At 550 °C, all ferritic steel samples showed corrosion. Pure KCl deposit induced the thickest oxide layer of 40 µm in the presence of HCl. However, with K-ilmenite$_{red,}$ a thin but noticeable corrosion layer was also measured on the austenitic TP347 sample. A similar corrosion layer was not detected on TP347 covered with the KCl deposit but not exposed to HCl.

The results also suggested that corrosion in the air reactor will not take place even at high temperatures of 700 °C since chlorine will not be present under those conditions. However, already a small slipstream containing KCl (g) and/or HCl/$Cl_2$, entering the air reactor can cause minor corrosion.

Interestingly, the potassium content (4 wt%) in heat-treated K-ilmenite$_{ox}$ particles induced minor corrosion in dry air at 700 °C., i.e., under conditions simulating the air reactor in CLC. However, the mean thickness of the corrosion layers was markedly thinner than reported for the same type of materials exposed to pure KCl at 600 °C in air by Wu et al. [34] and Lehmusto et al. [35]. Wu et al. [34] measured a mean corrosion thickness of 30 µm for TP347 and 57µm for S28, while Lehmusto et al. [35] reported a mean corrosion layer thickness of some 40 µm for alloy 625. The results suggest that the potassium content alone, with the negligible chloride content in the K-ilmenite$_{ox}$ deposit, does not lead to as severe corrosion as reported for pure KCl deposits.

The results indicate that ferritic steels are not suitable as heat exchanger materials under the reducing conditions in the fuel reactor if humidity and HCl are present in the atmosphere above 450 °C. The austenitic steels, again, withstand corrosion induced by potassium-containing deposits.

In contrast, in the oxidizing conditions of the air reactor at 700 °C, the austenitic steels showed no more corrosion than nickel-based alloys and would thus be suitable as a heat exchange material in the conditions studied.

The present study focused on the corrosive properties of one ash compound only. Interaction of KCl with other potassium salts or, e.g., calcium compounds and other oxygen carrier material may be of interest to study in the future.

## 5. Conclusions

The influence of potassium-contaminated ilmenite bed particles on corrosion of seven heat-exchanger materials was studied in laboratory furnaces under conditions simulating chemical-looping combustion of biomass. The experiments were carried out simulating both the air and fuel reactors. Heat-treated ilmenite, reduced K-doped ilmenite, re-oxidized K-doped ilmenite, and KCl were used as deposits on austenitic and ferritic steels and nickel-based alloys.

Under reducing conditions simulating the conditions experienced by a heat exchanger in the fuel reactor, the ferritic steels 10CrMo9-19 and X10 showed clear indications of corrosion at 450 °C both with and without deposits. At 550 °C, the corrosion was noticeable in all ferritic steel samples. Pure KCl deposits induced the thickest oxide layer in the presence of HCl.

The potassium content (4 wt%) in heat-treated ilmenite particles induced some corrosion in dry air at 700 °C., i.e., conditions simulating the air reactor in CLC.

The results indicate that ferritic steels are not suitable as heat exchanger materials under reducing conditions in the fuel reactor above 450 °C. The austenitic steels, again, can withstand corrosion induced by potassium-containing deposits.

Under oxidizing conditions in the air reactor at 700 °C, the austenitic steels showed no more corrosion than nickel-based alloys and were thus expected to be suitable as heat exchange materials in the conditions studied.

**Supplementary Materials:** The following supporting information can be downloaded at: https://www.mdpi.com/article/10.3390/en15082740/s1, Table S1: corrosion layer thickness values; Figures S1–S6 corrosion layer thickness distributions of air/fuel reactor tests.

**Author Contributions:** Conceptualization, A.B., M.Z., J.-E.E., P.Y. and L.H.; methodology J.-E.E., P.Y. and M.Z.; analyses, J.-E.E.; writing—original draft, J.-E.E.; writing—review and editing, M.Z., L.H., P.Y. and A.B.; supervision, L.H., M.Z., P.Y. and A.B.; project administration A.B. and M.Z.; funding acquisition, A.B. All authors have read and agreed to the published version of the manuscript.

**Funding:** This work was financed by Nordic Flagship Project no. 77732 "Negative CO2 emissions in the Nordic energy system" (2015–2019), funded by the Nordic Energy Research The APC was funded by Åbo Akademi University. The financial support by Åbo Akademi University is acknowledged.

**Institutional Review Board Statement:** Not applicable.

**Informed Consent Statement:** Not applicable.

**Data Availability Statement:** Not applicable.

**Acknowledgments:** Linus Silvander is acknowledged for the help with the SEM analyses.

**Conflicts of Interest:** The authors declare no conflict of interest.

## References

1. Masson-Delmotte, V.; Zhai, P.; Pörtner, H.O.; Roberts, D.; Skea, J.; Shukla, P.R.; Pirani, A.; Moufouma-Okia, W.; Péan, C.; Pidcock, R.; et al. *Global Warming of 1.5 °C. An IPCC Special Report on the Impacts of Global Warming of 1.5 °C above Pre-Industrial Levels and Related Global Greenhouse Gas Emission Pathways, in the Context of Strengthening the Global Response to the Threat of Climate Change, Sustainable Development, and Efforts to Eradicate Poverty*; IPCC: Geneva, Switzerland, 2018.
2. Azar, C.; Lindgren, K.; Obersteiner, M.; Riahi, K.; van Vuuren, D.P.; Den Elzen, K.M.G.J.; Möllersten, K.; Larson, E.D. The feasibility of low $CO_2$ concentration targets and the role of bio-energy with carbon capture and storage (BECCS). *Clim. Chang.* **2010**, *100*, 195–202. [CrossRef]
3. Lyngfelt, A.; Leckner, B.; Mattisson, T. A fluidized-bed combustion process with inherent $CO_2$ separation; application of chemical-looping combustion. *Chem. Eng. Sci.* **2001**, *56*, 3101–3113. [CrossRef]
4. Lewis, W.K.; Gilliland, E.R. Production of Pure Carbon Dioxide. U.S. Patent 2,665,972, 12 January 1954.
5. Ishida, M.; Jin, H. A new advanced power-generation system using chemical-looping combustion. *Energy* **1994**, *19*, 415–422. [CrossRef]
6. Lyngfelt, A. Chemical-looping combustion of solid fuels-status of development. *Appl. Energy* **2014**, *113*, 1869–1873. [CrossRef]
7. Lyngfelt, A. Chemical Looping Combustion: Status and Development Challenges. *Energy Fuels* **2020**, *34*, 9077–9093. [CrossRef]

8. Czakiert, T.; Krzywanski, J.; Zylka, A.; Nowak, W. Chemical Looping Combustion: A Brief Overview. *Energies* **2022**, *15*, 1563. [CrossRef]
9. Coppola, A.; Scala, F. Chemical Looping for Combustion of Solid Biomass: A Review. *Energy Fuels* **2021**, *35*, 19248–19265. [CrossRef]
10. Lyngfelt, A.; Linderholm, C. Chemical-Looping Combustion of Solid Fuels-Technology Overview and Recent Operational Results in 100 KW Unit. *Energy Procedia* **2014**, *63*, 98–112. [CrossRef]
11. Lyngfelt, A.; Leckner, B. 1000 MWth Boiler for Chemical-Looping Combustion of Solid Fuels–Discussion of Design and Costs. Appl. *Energy* **2015**, *157*, 475–487. [CrossRef]
12. Lyngfelt, A.; Brink, A.; Langørgen, Ø.; Mattisson, T.; Rydén, M.; Linderholm, C. 11,000 h of chemical-looping combustion operation—Where are we and where do we want to go? *Int. J. Greenh. Gas Control* **2019**, *88*, 38–56. [CrossRef]
13. Ryden, M.; Lyngfelt, A.; Langoergen, O.; Larring, Y.; Brink, A.; Teir, S.; Havaag, H.; Karmhagen, P. Negative $CO_2$ Emissions with Chemical-Looping Combustion of Biomass-A Nordic Energy Research Flagship Project. *Energy Procedia* **2017**, *114*, 6074–6082. [CrossRef]
14. Kluger, F.; Abdulally, I.; Andrus, H.; Levasseur, A.; Beal, B.; Marion, J. Overview of Alstom's Chemical Looping Programs. In Proceedings of the 5th Meeting of the IEAGHG International Oxyfuel Combustion Research Network, Wuhan, China, 28 October 2015.
15. Berguerand, N.; Lyngfelt, A. Batch testing of solid fuels with ilmenite in a 10 kW chemical-looping combustor. *Fuel* **2010**, *89*, 1749–1762. [CrossRef]
16. Thunman, H.; Lind, F.; Breitholtz, C.; Berguerand, N.; Seemann, M. Using an Oxygen-Carrier as Bed Material for Combustion of Biomass in a 12-MWth Circulating Fluidized-Bed Boiler. *Fuel* **2013**, *113*, 300–309. [CrossRef]
17. Cuadrat, A.; Abad, A.; Adanez, J.; de Diego, L.F.; Garcia-Labiano, F.; Gayan, P. Behavior of ilmenite as oxygen carrier in chemical-looping combustion. *Fuel Process Technol.* **2012**, *94*, 101–112. [CrossRef]
18. Knutsson, P.; Linderholm, C. Characterization of Ilmenite Used as Oxygen Carrier in a 100 KW Chemical-Looping Combustor for Solid Fuels. *Appl. Energy* **2015**, *157*, 368–373. [CrossRef]
19. Leion, H.; Lyngfelt, A.; Johansson, M.; Jerndal, E.; Mattisson, T. The use of ilmenite as an oxygen carrier in chemical-looping combustion. *Chem. Eng. Res. Des.* **2008**, *86*, 1017–1026. [CrossRef]
20. Zevenhoven, M.; Yrjas, P.; Skrifvars, B.-J.; Hupa, M. Characterization of Ash-Forming Matter in Various Solid Fuels by Selective Leaching and Its Implications for Fluidized-Bed Combustion. *Energy Fuels* **2012**, *26*, 6366–6386. [CrossRef]
21. Zevenhoven, M.; Yrjas, P.; Hupa, M. 14 Ash-Forming Matter and Ash-Related Problems. In *Handbook of Combustion*; Lackner, M., Winter, F., Agarwal, A.K., Eds.; Solid Fuels; Wiley-VCH Verlag GmbH & Co. KGaA: Weinheim, Germany, 2010; Volume 4, pp. 493–531.
22. Skrifvars, B.-J.; Backman, R.; Hupa, M.; Salmenoja, K.; Vakkilainen, E. Corrosion of superheater steel materials under alkali salt deposits. Part 1: The effect of salt deposit composition and temperature. *Corros. Sci.* **2008**, *50*, 1274–1282. [CrossRef]
23. Enestam, S.; Bankiewicz, D.P.; Tuiremo, J.; Makela, K.; & Hupa, M. Are NaCl and KCl equally corrosive on superheater materials of steam boilers? *Fuel* **2013**, *104*, 294–306. [CrossRef]
24. Wu, H.; Bankiewicz, D.; Yrjas, P.; Hupa, M. Laboratory Studies of Potassium-Halide-Induced High-Temperature Corrosion of Superheater Steels. Part 2: Exposures in Wet Air. *Energy Fuels* **2015**, *29*, 2709–2718. [CrossRef]
25. Elger, R. High Temperature Corrosion in Biomass-Fired Energy Applications: Alloying Effects and Test Environment Comparisons. Ph.D. Thesis, KTH Royal Institute of Technology, Stockholm, Sweden, 2016.
26. Larsson, E.; Liske, J.; Persdotter, A.; Jonsson, T.; Svensson, J.E.; Johansson, L.G. The Influence of KCl and HCl on the High-Temperature Oxidation of a Fe-2.25 Cr-1Mo Steel at 400 °C. *Oxid. Met.* **2020**, *93*, 29–52. [CrossRef]
27. Spiegel, M.; Zahs, A.; Grabke, H.J. Fundamental aspects of chlorine induced corrosion in power plants. *Mater. High Temp.* **2003**, *20*, 153–159. [CrossRef]
28. Cantatore, V.; Olivas Ogaz, M.A.; Liske, J.; Jonsson, T.; Svensson, J.E.; Johansson, L.G.; Panas, I. Oxidation driven permeation of Iron oxide scales by chloride from experiment guided first-principles modeling. *J. Phys. Chem. C* **2019**, *123*, 25957–25966. [CrossRef]
29. Pettersson, C.; Pettersson, J.; Asteman, H.; Svensson, J.E.; Johansson, L.G. KCl-induced high temperature corrosion of the austenitic Fe–Cr–Ni alloys 304L and Sanicro 28 at 600 °C. *Corros. Sci.* **2006**, *48*, 1368–1378. [CrossRef]
30. Lehmusto, J.; Yrjas, P.; Skrifvars, B.J.; Hupa, M. Detailed Studies on the High Temperature Corrosion Reactions between Potassium Chloride and Metallic Chromium. In *Materials Science Forum*; Trans Tech Publications Ltd.: Bachs, Switzerland, 2011; Volume 696, pp. 218–223.
31. Ruh, A.; Spiegel, M. Thermodynamic and kinetic consideration on the corrosion of Fe, Ni and Cr beneath a molten KCl–$ZnCl_2$ mixture. *Corros. Sci.* **2006**, *48*, 679–695. [CrossRef]
32. Jonsson, T.; Folkeson, N.; Halvarsson, M.; Svensson, J.E.; Johansson, L.G. Microstructural investigation of the HCl-induced corrosion of the austenitic alloy 310S (52Fe26Cr19Ni) at 500 °C. *Oxid. Met.* **2014**, *81*, 575–596. [CrossRef]
33. Bankiewicz, D.; Yrjas, P.; Hupa, M. High-temperature corrosion of superheater tube materials exposed to zinc salts. *Energy Fuels* **2009**, *23*, 3469–3474. [CrossRef]
34. Wu, H.; Yrjas, P.; Hupa, M. Laboratory Studies of Potassium-Halide-Induced High-Temperature Corrosion of Superheater Steels. Part 1: Exposures in Dry Air. *Energy Fuels* **2015**, *29*, 1186–1195. [CrossRef]

35. Lehmusto, J.; Yrjas, P.; Skrifvars, B.-J.; Hupa, M. High temperature corrosion of superheater steels by KCl and $K_2CO_3$ under dry andwet conditions. *Fuel Process. Technol.* **2012**, *104*, 253–264. [CrossRef]
36. Corcoran, A.; Marinkovic, J.; Lind, F.; Thunman, H.; Knutson, P.; Seeman, M. Ash properties of ilmenite used as bed material for combustion of biomass in a circulating Fluidized bed boiler. *Energy Fuels* **2014**, *28*, 7672–7679. [CrossRef]
37. Staničić, I.; Hanning, M.; Deniz, R.; Mattisson, T.; Backman, R.; Leion, H. Interaction of Oxygen Carriers with Common Biomass Ash Components. *Fuel Process. Technol.* **2020**, *200*, 106313. [CrossRef]
38. Zevenhoven, M.; Sevonius, C.; Salminen, P.; Lindberg, D.; Brink, A.; Yrjas, P.; Hupa, L. Defluidization of the Oxygen Carrier Ilmenite–Laboratory Experiments with Potassium Salts. *Energy* **2018**, *148*, 930–940. [CrossRef]
39. Hildor, F.; Zevenhoven, M.; Brink, A.; Hupa, L.; Leion, H. Understanding the Interaction of Potassium Salts with an Ilmenite Oxygen Carrier Under Dry and Wet Conditions. *ACS Omega* **2020**, *5*, 22966–22977. [CrossRef] [PubMed]
40. Bankiewicz, D. Corrosion Behaviour of Boiler Tube Materials during Combustion of Fuels Containing Zn and Pb. Ph.D. Thesis, Åbo Akademi University, Turku, Finland, 2012.
41. Gogolev, I.; Pikkarainen, T.; Kauppinen, J.; Linderholm, C.; Steenari, B.M.; Lyngfelt, A. Investigation of biomass alkali release in a dual circulating fluidized bed chemical looping combustion system. *Fuel* **2021**, *297*, 120743. [CrossRef]
42. Miao, Z.; Jiang, E.; Hu, Z. Review of agglomeration in biomass chemical looping technology. *Fuel* **2022**, *309*, 122199. [CrossRef]
43. Gogolev, I.; Soleimanisalim, A.H.; Linderholm, C.; Lyngfelt, A. Commissioning, performance benchmarking, and investigation of alkali emissions in a 10 kWth solid fuel chemical looping combustion pilot. *Fuel* **2021**, *287*, 119530. [CrossRef]